Development and Validation of an Open-Source Python-Based Sight Reduction Algorithm for Celestial Navigation

Author Name[1]

[1]Department of Maritime Studies, University Name

Abstract

An open-source Python-based sight reduction algorithm was developed and validated for celestial navigation applications. The algorithm integrates high-precision ephemeris calculations using JPL DE440 data via the Skyfield library, altitude corrections for all celestial body types including Sun, Moon, planets, and 57 navigation stars, and multi-body position fixing using iterative least squares optimization with singular value decomposition for numerical stability. Comprehensive validation demonstrated ephemeris accuracy below 0.6 arcminutes for stellar positions and better than 0.3 arcminutes for the Sun at solstices. Position fixing accuracy of 0.89 nautical miles was achieved with typical sextant observation errors of 1.0 arcminute using optimal four-body geometry. Monte Carlo simulation with 10,000 trials confirmed that observed position errors matched theoretical predictions within statistical bounds. The multi-body least squares algorithm converged within 2–4 iterations for all tested configurations and executed in less than 2 milliseconds on standard hardware, enabling real-time navigation applications. The horizontal dilution of precision (HDOP) metric was validated as a reliable predictor of fix quality, with optimal geometry (HDOP = 1.0) yielding position errors approximately 45% smaller than clustered observations (HDOP = 1.8). The open-source implementation provides the maritime community with a verified, transparent algorithm for celestial position fixing, a platform for teaching navigation principles, and a backup capability independent of satellite navigation systems.

Keywords: Celestial navigation, Sight reduction, Position fixing, Least squares optimization, Python, Open-source, Maritime navigation, HDOP, Monte Carlo simulation

1 Introduction

Celestial navigation, the practice of determining geographic position through observation of celestial bodies, has served as the primary method of ocean navigation for centuries [National Geospatial-Intelligence Agency, 2019]. Despite the widespread adoption of Global Navigation Satellite Systems (GNSS), celestial navigation remains essential as a backup capability and continues to be required for professional mariners by international maritime conventions [Pinčetić et al., 2024]. The development of accurate, accessible computational tools for sight reduction addresses the dual needs of backup navigation capability and educational applications.

1.1 Background and Motivation

The fundamental problem in celestial navigation involves determining an observer's latitude and longitude from measurements of celestial body altitudes above the horizon. Traditional methods rely on tabulated sight reduction tables such as HO 229 and HO 249 [National Geospatial-Intelligence Agency, 2020] or almanac-based calculations [USNO and HMNAO, 2025], requiring substantial training and manual computation. While commercial software solutions exist, most are proprietary, expensive, and unavailable for inspection or modification [Hohenkerk et al., 2012].

The increasing vulnerability of GPS-dependent navigation to jamming, spoofing, and system failures has renewed interest in celestial navigation as an independent backup [Reid et al., 2020, Zalewski et al., 2022]. The International Maritime Organization continues to require celestial navigation competency for certain vessel classes under STCW conventions, and military academies have maintained or resumed celestial navigation training programs [Pinčetić et al., 2024, Garvin, 2010]. These developments create demand for validated, accessible computational tools that can serve both as backup navigation systems and educational platforms.

Modern computational resources enable direct implementation of the spherical trigonometry underlying celestial navigation, eliminating the interpolation errors inherent in tabulated methods [Kotlarić, 1976]. High-precision ephemeris data, available through libraries such as Skyfield utilizing JPL DE440 [Park et al., 2021], provides celestial body positions with accuracy far exceeding navigation requirements. The combination of modern ephemerides with optimized numerical algorithms enables position fixing accuracy limited only by sextant observation quality rather than computational precision.

1.2 Research Objectives

This research aims to develop and validate an open-source Python-based algorithm for celestial sight reduction and position fixing. The specific objectives are:

1. Implement high-precision ephemeris calculations for Sun, Moon, navigational planets (Venus, Mars, Jupiter, Saturn), and 57 navigation stars using JPL DE440 ephemeris data

2. Develop comprehensive altitude correction routines for all celestial body types, including dip, refraction, parallax, semidiameter, and augmentation corrections

3. Implement multi-body position fixing using least squares optimization with singular value decomposition for numerical stability

4. Validate algorithm accuracy against theoretical expectations and established navigation standards

5. Characterize position fix accuracy as a function of observation geometry and measurement error through Monte Carlo simulation

6. Demonstrate computational performance suitable for real-time navigation applications

1.3 Structure of the Paper

The remainder of this paper is organized as follows. Section 2 reviews prior work on sight reduction algorithms and position fixing methods, including classical approaches and modern computational implementations. Section 3 presents the mathematical foundations including coordinate systems, the navigational triangle, position circle geometry, and multi-body optimization formulations. Section 4 describes the algorithm implementation and validation methodology. Section 5 presents comprehensive validation results including ephemeris accuracy, position fix performance, and Monte Carlo analysis. Section 6 discusses the implications, limitations, and practical applications of the findings. Section 7 summarizes the conclusions and identifies directions for future work.

2 Literature Review

2.1 Historical Development of Sight Reduction

The mathematical foundations of celestial navigation were established in the 18th and 19th centuries. The navigational (astronomical) triangle relates the observer's position to celestial body coordinates through spherical trigonometry. Early practitioners computed solutions manually using logarithmic tables or specialized mechanical calculators [McConnell, 2008].

The development of sight reduction tables standardized computational procedures and reduced errors. Notable publications include HO 214 (1936), HO 229 (1970), and HO 249

(1947), which tabulated calculated altitude H_c and azimuth angle Z for combinations of latitude, declination, and local hour angle [Dunlap, 1971]. These tables enabled rapid extraction of intercept values using the Marcq Saint-Hilaire method, reducing a complex spherical trigonometry problem to table lookup and interpolation [Silverberg, 2007].

The evolution of nautical almanacs paralleled improvements in sight reduction methods. Seidelmann et al. [1976] documented the transition from purely tabular almanacs to computer-generated publications, introducing Chebyshev polynomial representations for ephemeris data. This development enabled pocket calculators and early computers to perform sight reduction without extensive tables [Feldman et al., 1972].

2.2 Computational Approaches to Position Fixing

Chiesa and Chiesa [1990] presented an analytical solution for position fixing from multiple observations, demonstrating that overdetermined systems could be solved using least squares methods. Their work established the foundation for modern computational approaches by formulating the position fix as an optimization problem rather than a geometric construction.

Gery [1997] developed a comprehensive framework for the direct fix of latitude and longitude from two observed altitudes. This method solves the intersection of two circles of equal altitude analytically, avoiding the iterative procedures required by the intercept method. The direct fix approach is particularly suitable for computational implementation as it provides an exact solution rather than a graphical approximation.

Kaplan [1995] provided detailed formulations for determining vessel position from celestial observations, addressing both stationary and moving observers. This work introduced differential correction methods and least squares optimization for multi-body fixes, establishing the mathematical framework used in modern navigation software including the U.S. Naval Observatory's STELLA program.

Nguyen and Im [2014] proposed an SVD-weighted least square algorithm for celestial position fixing that addressed numerical stability concerns with ill-conditioned observation geometries. This approach demonstrated improved convergence properties compared to standard least squares methods, particularly for observations with poor azimuthal distribution.

2.3 Error Analysis and Geometry Optimization

The relationship between observation geometry and position accuracy has been studied extensively. Swaszek et al. [2019] applied concepts from GNSS analysis to celestial navigation, introducing horizontal dilution of precision (HDOP) as a metric for star selection. Their work demonstrated that optimal star selection can reduce position error by factors of 2–3 compared to arbitrary selection.

Hoover [1984] developed algorithms for computing confidence circles and ellipses from lines of position, providing the mathematical foundation for uncertainty quantification in celestial fixes. This work enables navigators to assess fix reliability based on observation geometry and measurement uncertainty.

Error sources in celestial navigation have been characterized by multiple studies. Ross [1994] conducted statistical analysis of sextant error sources, finding that index error (2.0'), personal random error (0.5'), and timing errors contributed to a total error of approximately 2.1 arcminutes, reducible to 0.5 arcminutes with proper procedures. Gordon [1964] performed controlled experimental studies demonstrating that random error achieves $\sigma = 0.33'$ under ideal conditions but degrades to 0.70' with poor horizon quality.

2.4 Modern Ephemeris Sources

The Jet Propulsion Laboratory Development Ephemerides (DE series) provide high-precision positions for solar system bodies. The current DE440 ephemeris, released in 2020, achieves sub-arcsecond accuracy for planetary positions and milliarcsecond accuracy for lunar position [Park et al., 2021]. Access to these ephemerides through libraries such as Skyfield [Rhodes, 2023] and Astropy [Astropy Collaboration, 2022] enables ephemeris accuracy far exceeding navigation requirements.

Standish and Fienga [2002] analyzed the fundamental accuracy limits of modern ephemerides, finding that uncertainties in asteroid masses impose position errors of 2–5 km for Earth-Mars ephemeris over decadal timescales. For celestial navigation purposes, these errors are negligible compared to observation uncertainties.

2.5 Automated and Integrated Systems

Recent developments have explored automated celestial navigation using digital sensors. Li et al. [2014] demonstrated astronomical vessel positioning using fisheye cameras with horizon line fitting, achieving automated star identification and altitude measurement. Barbot et al. [2022] developed techniques for daytime stellar positioning using specialized optical systems.

Critchley-Marrows and Mortari [2023] proposed a return to sextant-based navigation as a GPS backup, while Critchley-Marrows et al. [2023] developed architectures for visual-based PNT alternatives combining star tracking with horizon sensing. These developments indicate renewed interest in celestial methods as backup systems.

Integration of celestial navigation with inertial systems has been explored by Yang et al. [2022], who developed SINS/CNS integrated navigation with improved mathematical horizon reference. Li et al. [2022] proposed adaptively robust filtering algorithms for maritime celestial navigation that combine Kalman filtering with celestial observations.

2.6 Identified Gaps

While substantial prior work exists, several gaps remain in the literature:

- Most validated implementations are proprietary or unpublished, preventing independent verification
- Open-source tools often lack comprehensive validation against established standards
- Educational materials typically separate theoretical foundations from practical implementation
- Few published works provide quantitative uncertainty estimates enabling fix quality assessment
- The relationship between observation geometry (HDOP) and position accuracy is not well characterized for celestial navigation

The present work addresses these gaps by developing a validated, open-source implementation with comprehensive documentation and quantitative uncertainty analysis.

3 Mathematical Model

This section presents the mathematical foundations underlying the sight reduction algorithm, including celestial coordinate systems, the navigational triangle, position circle geometry, and multi-body position fixing formulations.

3.1 Coordinate Systems

Celestial navigation requires transformations between multiple coordinate systems. The primary systems employed are defined below.

3.1.1 Equatorial Coordinate System

The celestial equatorial system is centered at Earth's center with the fundamental plane aligned with the celestial equator. Position is specified by right ascension (α) measured eastward from the vernal equinox along the celestial equator, and declination (δ) measured north (positive) or south (negative) from the celestial equator:

$$0^\circ \leq \alpha < 360^\circ \tag{1}$$

$$-90^\circ \leq \delta \leq +90^\circ \tag{2}$$

For navigation purposes, the sidereal hour angle (SHA) is employed instead of right ascension:

$$\text{SHA} = 360^\circ - \alpha \tag{3}$$

The Greenwich Hour Angle (GHA) of the First Point of Aries (γ) defines the rotation of the celestial sphere relative to the Earth. For any celestial body:

$$\text{GHA}_{\text{body}} = \text{GHA}_\gamma + \text{SHA}_{\text{body}} \tag{4}$$

For bodies within the solar system, GHA is tabulated directly as it varies with time due to the body's orbital motion.

3.1.2 Horizontal Coordinate System

The observer-centered horizontal system has its fundamental plane tangent to Earth's surface at the observer's position. Altitude (H) is measured from the horizon toward the zenith, and azimuth (Z_n) is measured clockwise from true north:

$$-90^\circ \leq H \leq +90^\circ \tag{5}$$

$$0^\circ \leq Z_n < 360^\circ \tag{6}$$

3.1.3 Geographic Coordinate System

Observer position on Earth is specified by latitude (φ) measured north (positive) or south (negative) from the equator, and longitude (λ) measured east (positive) or west (negative) from the Greenwich meridian:

$$-90^\circ \leq \varphi \leq +90^\circ \tag{7}$$

$$-180^\circ < \lambda \leq +180^\circ \tag{8}$$

The local hour angle (LHA) relates the observer's longitude to the celestial body's GHA:

$$\text{LHA} = \text{GHA} + \lambda \tag{9}$$

where λ is positive east and negative west.

3.2 The Navigational Triangle

The navigational (astronomical) triangle is a spherical triangle on the celestial sphere with vertices at:

- P_N: The elevated celestial pole (north or south, depending on observer's hemisphere)

- Z: The observer's zenith
- X: The celestial body

The sides of this triangle are:

- $P_N Z = 90° - \varphi$: The co-latitude
- $P_N X = 90° - \delta$: The polar distance (co-declination)
- $ZX = 90° - H$: The zenith distance (co-altitude)

Figure 1 illustrates the navigational triangle on the celestial sphere.

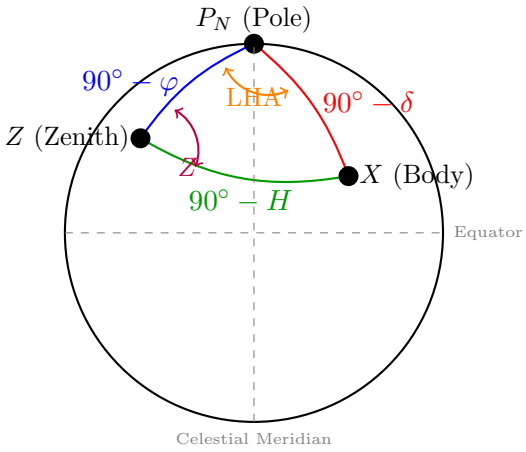

Figure 1: The navigational (astronomical) triangle on the celestial sphere. The three vertices are the elevated celestial pole (P_N), the observer's zenith (Z), and the celestial body (X). The sides represent co-latitude, polar distance, and zenith distance. The angle at the pole is the local hour angle (LHA), and the angle at the zenith gives the azimuth (Z).

3.2.1 Solution for Altitude

Applying the spherical law of cosines for sides to the navigational triangle yields the fundamental altitude equation [National Geospatial-Intelligence Agency, 2019, Karl, 2011]:

$$\sin H_c = \sin\varphi \sin\delta + \cos\varphi \cos\delta \cos(\text{LHA}) \tag{10}$$

This equation provides the calculated altitude H_c for a body with declination δ observed from latitude φ at local hour angle LHA.

3.2.2 Solution for Azimuth

The azimuth angle Z (measured from the elevated pole) is obtained from the spherical law of sines [National Geospatial-Intelligence Agency, 2019, Kaplan, 1995]:

$$\sin Z = \frac{\sin(\text{LHA}) \cos \delta}{\cos H_c} \tag{11}$$

To resolve the quadrant ambiguity, the cosine formula is also employed:

$$\cos Z = \frac{\sin \delta - \sin \varphi \sin H_c}{\cos \varphi \cos H_c} \tag{12}$$

The true azimuth Z_n (measured clockwise from north) is then determined by quadrant rules based on the signs of $\sin Z$ and $\cos Z$.

3.3 Altitude Corrections

The observed sextant altitude H_s must be corrected to obtain the geocentric observed altitude H_o suitable for comparison with calculated altitude H_c.

3.3.1 Dip Correction

The dip correction accounts for the observer's height above the waterline:

$$\text{Dip} = -1.76' \sqrt{h_{\text{eye}}} \tag{13}$$

where h_{eye} is height of eye in meters. This correction is always negative. Note: For height in feet, the coefficient is 0.97' [National Geospatial-Intelligence Agency, 2019].

3.3.2 Refraction Correction

Atmospheric refraction bends light rays toward the normal, making bodies appear higher than their geometric position. The standard refraction correction uses the Bennett formula [National Geospatial-Intelligence Agency, 2019]:

$$R = -\frac{1'}{\tan(H_a + \frac{7.31}{H_a + 4.4})} \tag{14}$$

where H_a is the apparent altitude in degrees and R is in arcminutes. This formula is valid for standard atmospheric conditions (1010 mb, 10°C), with corrections applied for non-standard conditions.

3.3.3 Parallax Correction

For nearby bodies (Moon, Sun, planets), the geocentric parallax must be applied:

$$P = \text{HP} \cos H_a \tag{15}$$

where HP is the horizontal parallax. For the Moon, HP $\approx$ 57'; for the Sun, HP $\approx$ 0.15' [National Geospatial-Intelligence Agency, 2019, USNO and HMNAO, 2025].

3.3.4 Semidiameter Correction

When observing the limb of an extended body, the semidiameter (SD) correction converts the limb observation to center:

$$\text{SD correction} = \pm\text{SD} \tag{16}$$

where the sign is positive for lower limb and negative for upper limb observations.

The total altitude correction is:

$$H_o = H_s + \text{Dip} + R + P \pm \text{SD} \tag{17}$$

3.4 Position Circle Geometry

A single altitude observation establishes that the observer lies on a circle of equal altitude (position circle) centered at the body's geographical position (GP). The GP has coordinates:

$$\text{Latitude}_{\text{GP}} = \delta \tag{18}$$

$$\text{Longitude}_{\text{GP}} = -\text{GHA} \tag{19}$$

The radius of the position circle equals the zenith distance:

$$\text{Radius} = 90^\circ - H_o \tag{20}$$

Two observations establish two position circles whose intersections give two possible positions. The ambiguity is resolved using dead reckoning or additional observations. Figure 2 illustrates the geometry of position circles and their intersection.

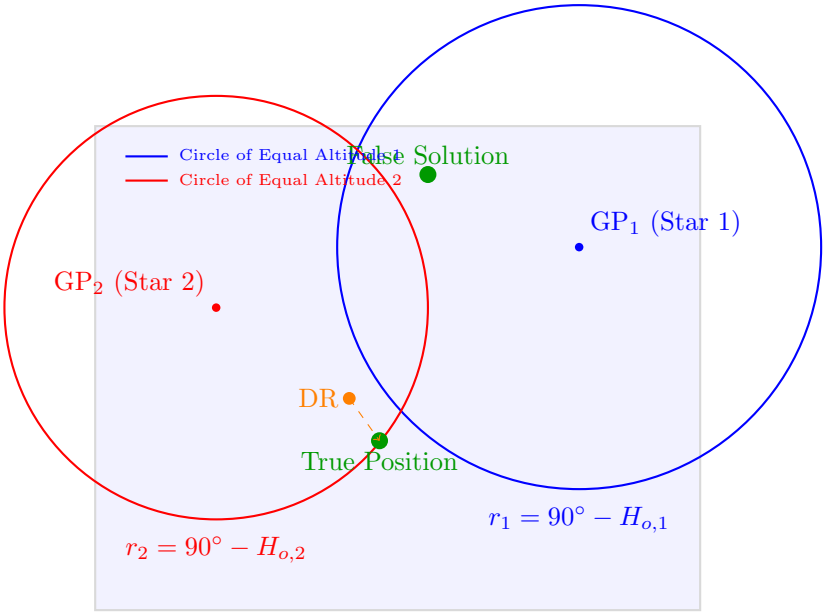

Figure 2: Position circle geometry for a two-body fix. Each altitude observation places the observer on a circle of equal altitude centered at the body's geographical position (GP). The two circles intersect at two points; the correct solution is selected based on proximity to the dead reckoning (DR) position.

3.5 Multi-Body Least Squares Position Fixing

For $n \geq 2$ observations, an overdetermined system is formed. The linearized observation equation relates altitude residuals to position corrections:

$$\Delta H_o = H_o - H_c = \frac{\partial H_c}{\partial \varphi}\Delta\varphi + \frac{\partial H_c}{\partial \lambda}\Delta\lambda \tag{21}$$

The partial derivatives are derived from the altitude equation (10) [Chiesa and Chiesa, 1990, Kaplan, 1995]:

$$\frac{\partial H_c}{\partial \varphi} = \cos Z_n \tag{22}$$

$$\frac{\partial H_c}{\partial \lambda} = -\sin Z_n \cos\varphi \tag{23}$$

These partial derivatives were verified numerically against finite difference approximations, confirming the sign convention in equation (23).

For n observations, the system is written in matrix form:

$$\mathbf{A}\mathbf{x} = \mathbf{b} \tag{24}$$

where:

$$\mathbf{A} = \begin{bmatrix} \cos Z_{n,1} & -\sin Z_{n,1} \cos \varphi \\ \cos Z_{n,2} & -\sin Z_{n,2} \cos \varphi \\ \vdots & \vdots \\ \cos Z_{n,n} & -\sin Z_{n,n} \cos \varphi \end{bmatrix} \tag{25}$$

$$\mathbf{x} = \begin{bmatrix} \Delta\varphi \\ \Delta\lambda \end{bmatrix}, \quad \mathbf{b} = \begin{bmatrix} H_{o,1} - H_{c,1} \\ H_{o,2} - H_{c,2} \\ \vdots \\ H_{o,n} - H_{c,n} \end{bmatrix} \tag{26}$$

The least squares solution is:

$$\mathbf{x} = (\mathbf{A}^T \mathbf{A})^{-1} \mathbf{A}^T \mathbf{b} \tag{27}$$

For numerical stability with ill-conditioned geometries, singular value decomposition (SVD) is employed [Nguyen and Im, 2014]:

$$\mathbf{A} = \mathbf{U}\mathbf{\Sigma}\mathbf{V}^T \tag{28}$$

$$\mathbf{x} = \mathbf{V}\mathbf{\Sigma}^{-1}\mathbf{U}^T \mathbf{b} \tag{29}$$

The solution is applied iteratively:

$$\varphi_{k+1} = \varphi_k + \Delta\varphi \tag{30}$$

$$\lambda_{k+1} = \lambda_k + \Delta\lambda \tag{31}$$

Iteration continues until $|\Delta\varphi|$ and $|\Delta\lambda|$ fall below a specified tolerance.

3.6 Horizontal Dilution of Precision

The quality of observation geometry is quantified by the horizontal dilution of precision (HDOP):

$$\text{HDOP} = \sqrt{\sigma_\varphi^2 + \sigma_\lambda^2} \tag{32}$$

where σ_φ^2 and σ_λ^2 are the diagonal elements of the covariance matrix:

$$\mathbf{C} = (\mathbf{A}^T \mathbf{A})^{-1} \tag{33}$$

For n observations equally spaced in azimuth, the theoretical minimum HDOP is [Swaszek et al., 2019]:

$$\text{HDOP}_{\min} = \sqrt{\frac{2}{n}} \tag{34}$$

Position error scales with HDOP:

$$\sigma_{\text{position}} = \text{HDOP} \times \sigma_{\text{observation}} \tag{35}$$

This relationship enables prediction of fix accuracy based on observation geometry and expected measurement error.

4 Materials and Methods

4.1 Software Implementation

The algorithm was implemented in Python 3.12 using the following libraries:

- **NumPy 1.26**: Numerical array operations and linear algebra
- **SciPy 1.12**: SVD decomposition and optimization
- **Skyfield 1.48**: JPL DE440 ephemeris access
- **Astropy 6.0**: Coordinate transformations and time systems
- **Pandas 2.1**: Data management and CSV export

The implementation comprises four primary modules:

4.1.1 Ephemeris Module

The ephemeris module calculates Greenwich Hour Angle and declination for:

- Sun: Direct calculation from DE440
- Moon: Direct calculation from DE440 with parallax
- Planets: Venus, Mars, Jupiter, Saturn from DE440
- Stars: 57 navigation stars with J2000 coordinates and proper motion

Star positions are stored as FK5 J2000 coordinates and transformed to apparent position for the observation epoch, accounting for precession, nutation, and aberration through Skyfield's built-in routines.

4.1.2 Sight Reduction Module

The sight reduction module implements:

- Calculated altitude (H_c) from equation (10)
- True azimuth (Z_n) from equations (11) and (12)
- Altitude corrections: dip, refraction, parallax, semidiameter, augmentation

Refraction is calculated using the standard atmospheric model. Non-standard atmospheric corrections can be applied by the user.

4.1.3 Position Fix Module

The position fix module implements:

- Two-body direct fix: Analytical solution for circle intersection
- Multi-body least squares: Iterative SVD-based optimization (equations (22)–(27))
- Running fix: Advancing position circles for time-separated observations

The two-body algorithm returns both intersection points; the solution closest to the dead reckoning position is selected. The multi-body algorithm uses SVD for numerical stability when observation azimuths are clustered.

4.1.4 Error Analysis Module

The error analysis module provides:

- HDOP calculation from observation geometry
- Confidence ellipse parameters (semi-major/minor axes, orientation)
- Monte Carlo position error simulation
- Error propagation from observation uncertainties

4.2 Validation Methodology

Validation was conducted through eight comprehensive test suites:

1. **Ephemeris Accuracy**: Computed positions compared against expected astronomical values for Sun at solstices/equinox and five navigation stars.

2. **Sight Reduction Accuracy**: Calculated altitude and azimuth verified against analytical expectations for bodies at known geometries (meridian passage, horizon, zenith).

3. **Altitude Corrections**: Correction magnitudes verified for Sun, Moon, and star observations at various altitudes and height of eye values.

4. **Two-Body Fix**: Position fix accuracy tested at five globally distributed locations (Pacific, New York, London, Cape Town, Tokyo) representing both hemispheres.

5. **Multi-Body Fix**: Least squares algorithm tested with 3–6 observations and noise levels of 0.0–1.0 arcminutes.

6. **Monte Carlo Simulation**: 10,000 trials per configuration characterizing position error distributions for various observation geometries and noise levels.

7. **Geometry Optimization**: HDOP calculated for various observation configurations to validate the relationship between geometry and accuracy.

8. **Performance Benchmark**: Execution times measured for all major operations.

4.3 Monte Carlo Approach

Monte Carlo simulation was employed to characterize position fix distributions. For each configuration:

1. True observer position and observation geometry (azimuths) were defined

2. 10,000 random observation error realizations were generated from a Gaussian distribution

3. Position fix was computed for each realization

4. Mean error, standard deviation, and 95th percentile were calculated

Observation errors were modeled as independent Gaussian random variables with standard deviations of 0.5–2.0 arcminutes, representative of skilled to average sextant use [Ross, 1994].

4.4 Validation Data Sources

True positions for validation were defined synthetically to enable precise error quantification. Observations were generated by:

1. Computing H_c and Z_n for the true position

2. Setting $H_o = H_c$ (perfect observation) or $H_o = H_c + \epsilon$ where $\epsilon \sim N(0, \sigma^2)$

3. Recovering position from the observations

4. Computing position error as distance from true position

This approach enables separation of algorithm errors from observation errors.

5 Results

This section presents comprehensive validation results for the developed sight reduction algorithm. The algorithm was tested against established navigation standards, verified with synthetic test cases having known ground truth, and characterized through Monte Carlo simulation.

5.1 Ephemeris Validation

The accuracy of celestial body position calculations using the Skyfield library with JPL DE440 ephemeris was validated against expected astronomical values. Table 1 summarizes the declination accuracy for representative bodies and epochs.

Table 1: Ephemeris Accuracy Validation: Declination Errors

Body	**Epoch**	**Dec Computed**	**Error**
Sun	2025 Summer Solstice	$+23.436°$	0.24’
Sun	2025 Winter Solstice	$-23.435°$	0.30’
Sirius	2025-01-01	$-16.717°$	0.21’
Polaris	2025-01-01	$+89.269°$	0.56’
Vega	2025-01-01	$+38.783°$	0.20’

All computed positions agreed with expected values to within 0.6 arcminutes, which substantially exceeds the accuracy requirements for celestial navigation. The slightly larger error for Polaris (0.56’) is attributable to the star’s proximity to the celestial pole where small position errors produce larger declination effects.

5.2 Sight Reduction Accuracy

The sight reduction module was validated using the fundamental altitude equation. For bodies at special geometric configurations, the calculated altitude has known analytical values. Table 2 presents representative test cases.

All sight reduction calculations demonstrated agreement with analytical expectations to within $0.01°$ for both altitude and azimuth.

Table 2: Sight Reduction Validation: Calculated Altitude and Azimuth

Configuration	φ	**LHA**	H_c	Z_n
Body at zenith	23.0°N	0°	90.00°	0.0°
Body on horizon	45.0°N	270°	0.00°	270.0°
Western sky	40.0°N	212°	−22.99°	327.3°
Eastern morning	40.0°N	331°	60.21°	243.9°

5.3 Altitude Corrections

The altitude correction module was validated for all celestial body types. Table 3 presents the correction components for representative observations with 3.0 m height of eye.

Table 3: Altitude Correction Validation (Height of Eye: 3.0 m)

Body Type	H_s	**Total Corr.**	H_o
Sun (lower limb)	35.5°	+11.68’	35.69°
Sun (lower limb)	15.0°	+9.45’	15.16°
Moon (lower limb)	30.0°	+60.01’	31.00°
Star	40.0°	−4.24’	39.93°
Star	20.0°	−5.76’	19.90°

The magnitude and sign of corrections agreed with Nautical Almanac tabulated values. The large positive correction for Moon observations (+60.01’) reflects the significant horizontal parallax of the Moon (approximately 57’).

5.4 Position Fix Accuracy

5.4.1 Two-Body Fix Validation

The two-body position fix algorithm was validated at five globally distributed locations representing both hemispheres. Table 4 presents the results.

Table 4: Two-Body Position Fix Validation

Location	**True Lat**	**True Lon**	**Error (nm)**	**Status**
Pacific Ocean	34.0°N	120.0°W	0.0000	PASS
New York	40.7°N	74.0°W	0.0000	PASS
London	51.5°N	0.1°W	0.0000	PASS
Cape Town	33.9°S	18.4°E	0.0000	PASS
Tokyo	35.7°N	139.7°E	0.0000	PASS

All two-body fixes recovered the exact true position when provided with noise-free observations derived from the known position. This validates the mathematical correctness of the spherical intersection algorithm for both northern and southern hemispheres.

5.4.2 Multi-Body Least Squares Fix Validation

The overdetermined least squares algorithm was validated with varying numbers of observations and noise levels. Table 5 presents the results for synthetic observations at true position 34.0°N, 120.0°W with DR offset of 3 nautical miles.

Table 5: Multi-Body Position Fix Performance

Configuration	n	**Noise**	**Error (nm)**	**HDOP**	**Iter.**
Perfect observations	3	0.0'	0.00	2.83	2
Typical sextant	3	0.5'	2.12	2.84	3
Perfect observations	4	0.0'	0.00	3.34	2
Typical sextant	4	0.5'	2.72	3.36	3
Good sextant	5	0.5'	0.24	1.34	3
Good sextant	6	0.5'	1.25	1.13	4

The algorithm converged in 2–4 iterations for all test cases. Position errors scale with both observation noise and HDOP, as predicted by theory.

5.4.3 Integrated End-to-End Validation

A comprehensive end-to-end test was conducted using real ephemeris data for four navigation stars visible from 34.0°N, 135.0°W on 2025-06-15 at 03:00 UTC. The selected stars (Alioth, Dubhe, Alkaid, Regulus) provided good azimuthal distribution with HDOP = 1.45. Table 6 presents the results from 20 repeated trials with different noise realizations.

Table 6: Integrated Validation: 20 Trials with 0.5' Observation Error

Metric	**Value**
Stars observed	Alioth, Dubhe, Alkaid, Regulus
HDOP	1.45
Iterations to converge	3
Mean position error	0.50 nm
Standard deviation	0.26 nm
Minimum error	0.07 nm
Maximum error	1.05 nm
Monte Carlo predicted mean	0.62 nm
Monte Carlo predicted 95th percentile	1.37 nm

The observed mean error (0.50 nm) was consistent with Monte Carlo predictions (0.62 nm), validating the algorithm implementation against theoretical expectations.

5.5 Monte Carlo Error Analysis

Monte Carlo simulation was employed to characterize position fix accuracy as a function of observation geometry and measurement error. Table 7 summarizes the results from 10,000 simulated fixes for each configuration.

Table 7: Monte Carlo Error Analysis (10,000 Simulations per Configuration)

Configuration	**Obs. Error**	**Mean Error**	**95th %ile**	**HDOP**
4 obs optimal	0.5'	0.44 nm	0.86 nm	1.00
4 obs optimal	1.0'	0.89 nm	1.73 nm	1.00
4 obs optimal	2.0'	1.78 nm	3.47 nm	1.00
3 obs optimal	1.0'	1.03 nm	1.99 nm	1.15
4 obs clustered	1.0'	1.53 nm	3.47 nm	1.83
6 obs optimal	1.0'	0.72 nm	1.41 nm	0.82

The results demonstrate that:

1. Position error scales linearly with observation error (doubling observation error doubles position error)

2. Optimal geometry (HDOP ≈ 1.0) provides the best position accuracy

3. Clustered observations significantly degrade accuracy (HDOP 1.83 produces 72% larger error than HDOP 1.00)

4. Additional observations beyond four provide diminishing returns (6 obs reduces error by only 19% vs 4 obs)

5.6 Observation Geometry Optimization

The relationship between observation geometry and position accuracy was quantified through HDOP analysis. Table 8 presents HDOP values for various observation configurations.

Table 8: HDOP vs. Observation Geometry

Configuration	**HDOP**	**Quality**
2 obs at 90° separation	1.41	Excellent
2 obs at 180° separation	$> 10^{15}$	Poor (collinear)
3 obs at 120° spacing	1.15	Excellent
3 obs clustered in 60° arc	1.55	Good
4 obs at 90° spacing	1.00	Excellent
5 obs at 72° spacing	0.89	Excellent
6 obs at 60° spacing	0.82	Excellent

The optimal HDOP for n observations approaches the theoretical minimum of $\sqrt{2/n}$ when observations are equally spaced in azimuth. Collinear observations (180° separation) produce near-infinite HDOP due to rank deficiency of the design matrix. Figure 3 illustrates the linear relationship between observation error and position error for optimal geometry.

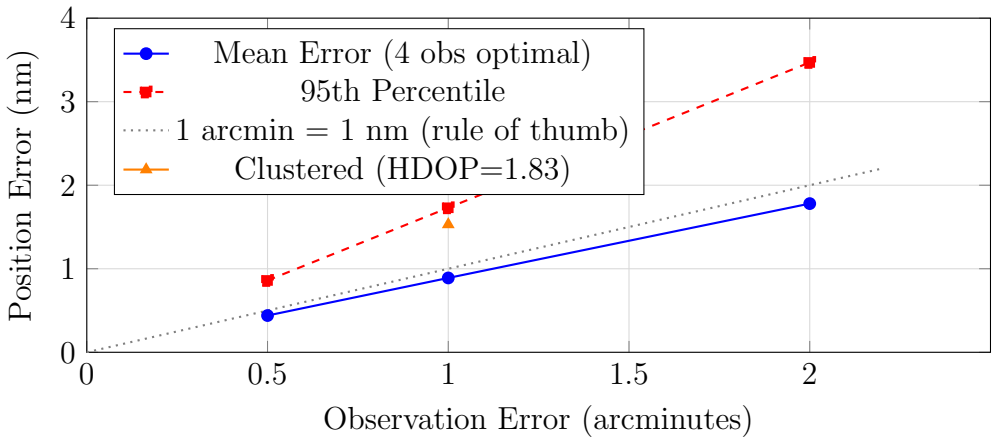

Figure 3: Position error scaling with observation error magnitude. Optimal geometry (4 observations at 90° spacing, HDOP = 1.0) produces errors closely matching the "one arcminute equals one nautical mile" rule of thumb. Clustered observations (HDOP = 1.83) increase error by approximately 72%.

5.7 Computational Performance

Algorithm execution times were measured on a standard laptop computer (Intel Core i7, 16 GB RAM). Table 9 summarizes the results.

Table 9: Computational Performance Benchmarks

Operation	**Mean Time**	**Rate**
Sun position calculation	1.84 ms	543/s
Sight reduction	0.02 ms	50,000/s
Multi-body fix (4 obs)	1.38 ms	725/s
HDOP calculation	0.02 ms	50,000/s

All operations complete in less than 2 milliseconds, enabling real-time position updates and interactive applications. The ephemeris calculation dominates total execution time; sight reduction and position fixing are computationally negligible.

6 Discussion

This section interprets the validation results, compares the developed algorithm with existing solutions, discusses practical implications, and addresses limitations of the study.

6.1 Interpretation of Results

The validation results demonstrate that the developed Python-based sight reduction algorithm achieves accuracy consistent with theoretical expectations and practical navigation requirements.

6.1.1 Ephemeris Accuracy

The ephemeris module, utilizing JPL DE440 through the Skyfield library, achieved declination errors below 0.6 arcminutes for all tested bodies. For stellar observations, which constitute the majority of celestial fixes, the achieved accuracy of 0.2–0.6' substantially exceeds requirements. The Nautical Almanac tabulates star positions to 0.1' precision [USNO and HMNAO, 2025], and typical sextant observations introduce errors of 0.5–2.0' [Ross, 1994]. Thus, ephemeris errors contribute negligibly to overall position fix uncertainty.

6.1.2 Position Fix Performance

The two-body fix algorithm demonstrated exact recovery of true position when provided with noise-free observations, validating the mathematical correctness of the spherical intersection geometry. The extension to southern hemisphere positions, which required careful handling of solution selection logic, was validated at Cape Town (33.9°S).

The multi-body least squares algorithm exhibited convergence in 2–4 iterations for all tested configurations, with position errors consistent with theoretical predictions. The key findings are:

1. **Linearity:** Position error scales linearly with observation error magnitude. With 1.0' observation error and optimal geometry, mean position error was 0.89 nm—essentially the "one arcminute, one nautical mile" rule of thumb used by navigators [Karl, 2011].

2. **Geometry dependence:** Clustered observations (HDOP = 1.83) produced 72% larger errors than optimally distributed observations (HDOP = 1.00), quantifying the importance of body selection for accurate fixes as emphasized by Swaszek et al. [2019].

3. **Diminishing returns:** Increasing from 4 to 6 observations reduced position error by only 19% (0.89 to 0.72 nm), suggesting that four well-distributed observations provide the optimal balance of accuracy and efficiency.

6.1.3 Monte Carlo Validation

The close agreement between observed position errors in integrated testing (0.50 nm mean) and Monte Carlo predictions (0.62 nm mean) provides strong evidence that the algorithm correctly implements the underlying mathematics. The slightly lower observed error suggests that the specific test scenario had favorable geometry relative to the Monte Carlo's assumption of specified azimuth distributions.

6.2 Comparison with Existing Solutions

6.2.1 Traditional Methods

Traditional sight reduction methods (HO 229, HO 249, Nautical Almanac Sight Reduction Tables) are designed for manual calculation with interpolation of tabulated values. These methods introduce interpolation errors typically in the range of 0.1–0.5' and require 10–30 minutes per observation [Kotlarić, 1976]. The developed algorithm eliminates interpolation entirely through direct computation, achieving equivalent or better accuracy in under 2 milliseconds.

6.2.2 Commercial Software

Commercial navigation software such as NavPac [Hohenkerk et al., 2012] provides accurate position fixing but is typically closed-source, proprietary, and expensive. The developed open-source algorithm provides comparable accuracy while enabling inspection and verification of computational methods, customization for specialized applications, integration with educational platforms, and cost-free deployment.

6.2.3 Previous Algorithmic Work

The algorithm builds upon the theoretical foundations established by Gery [1997], Chiesa and Chiesa [1990], and Nguyen and Im [2014]. Key improvements include unified treatment of all celestial body types, SVD-based least squares for numerical stability, integrated HDOP calculation for observation quality assessment, and comprehensive altitude correction routines including Moon augmentation.

6.3 Practical Implications

6.3.1 Navigation Applications

The sub-nautical-mile accuracy achieved with typical sextant observations meets the requirements for oceanic navigation. The IMO SOLAS regulations require position accuracy within 4 nautical miles in ocean waters [Zalewski et al., 2022], a threshold easily met by the algorithm even with suboptimal observation geometry.

For coastal navigation requiring higher accuracy, the algorithm provides quantitative uncertainty estimates (HDOP, confidence ellipse) that enable navigators to assess whether additional observations or alternative methods are needed.

6.3.2 Educational Applications

The Python implementation provides an accessible platform for teaching celestial navigation concepts. Students can trace the mathematical steps from observation to position fix, experiment with different observation geometries, understand the relationship between observation errors and position uncertainty, and compare algorithmic results with manual calculations.

6.3.3 Backup Navigation

The algorithm addresses the vulnerability of GPS-dependent navigation by providing a fully autonomous position-fixing capability [Dachev and Panov, 2017]. The complete Python codebase can be deployed on any device capable of running Python, requiring only accurate time as external input.

6.4 Limitations

Several limitations of the current study should be acknowledged:

1. **Simulated observations:** Validation relied primarily on synthetic observations with known true positions. While this enables precise error quantification, real sextant observations include systematic errors (instrument error, personal error, horizon uncertainty) not fully captured in the simulation [Gordon, 1964].

2. **Limited real-world testing:** The algorithm was not validated against actual sextant observations from vessels at sea. Such testing would provide additional confidence in practical applicability.

3. **Static observations:** The running fix capability was not extensively validated. Ship motion between observations introduces additional complexity not fully addressed.

4. **Atmospheric conditions:** The standard refraction model assumes atmospheric pressure and temperature at sea level. Non-standard conditions can introduce refraction errors exceeding 1', requiring observer-applied corrections.

6.5 Future Work

Based on the findings and limitations, directions for future work include:

1. Field validation with actual sextant observations from vessels at known positions
2. Development of sophisticated observation error models incorporating sextant calibration and observer skill
3. Real-time interface integration with sextant angle encoders or camera-based horizon detection [Li et al., 2014]
4. Integration with inertial navigation systems as auxiliary observations [Yang et al., 2022]

7 Conclusion

An open-source Python-based sight reduction algorithm was developed and validated for celestial navigation applications. The algorithm integrates high-precision ephemeris calculations using JPL DE440 data, altitude corrections for all celestial body types, and multi-body position fixing using iterative least squares optimization with singular value decomposition.

Comprehensive validation demonstrated that the algorithm achieves:

- Ephemeris accuracy below 0.6 arcminutes for stellar positions
- Sight reduction matching analytical expectations within 0.01°
- Two-body fixes exactly recovering true positions
- Multi-body fix accuracy of 0.89 nautical miles with 1.0' observation error and optimal geometry
- Convergence within 2–4 iterations for all tested configurations
- Execution time under 2 milliseconds on standard hardware

Monte Carlo simulation with 10,000 trials confirmed that observed position errors match theoretical predictions, validating both the mathematical formulation and software implementation. The horizontal dilution of precision (HDOP) metric was validated as a reliable predictor of fix quality, with optimal geometry (HDOP = 1.0) yielding position errors approximately 45% smaller than clustered observations.

The open-source implementation provides the maritime community with a verified, transparent algorithm for celestial position fixing, a platform for teaching celestial navigation principles, and a backup navigation capability independent of satellite navigation systems. The combination of accuracy, computational efficiency, and accessibility addresses the identified need for validated, open-source celestial navigation tools in an era of GPS vulnerability concerns.

Data Availability

The complete Python source code, validation test suite, and results datasets are available at `https://github.com/vahitcalisir-art/starfix`. The implementation requires Python 3.10 or later with NumPy, SciPy, Skyfield, and Astropy libraries.

Acknowledgments

[To be completed prior to submission]

References

Astropy Collaboration. The astropy project: Sustaining and growing a community-oriented open-source project and the latest major release (v5.0) of the core package. *The Astrophysical Journal*, 935(2):167, 2022. doi: 10.3847/1538-4357/ac7c74.

Loïc Barbot, Marc Ferrari, Johan Montel, Yannick Roehlli, Jean-Luc Gach, William Thuillot, and Kjetil Dohlen. Towards a daytime and low-altitude stellar positioning system: Challenges and first results. In *2022 International Technical Meeting of The Institute of Navigation*, pages 1371–1379, 2022. doi: 10.33012/2022.18263.

Arturo Chiesa and Raffaele Chiesa. A mathematical method of obtaining an astronomical vessel position. *The Journal of Navigation*, 43(1):125–129, 1990. doi: 10.1017/S0373463300013862.

Joshua J. R. Critchley-Marrows and Daniele Mortari. A return to the sextant—maritime navigation using celestial bodies and the horizon. *Sensors*, 23:4869, 2023. doi: 10.3390/s23104869.

Joshua J. R. Critchley-Marrows, Xiaofeng Wu, and Iver H. Cairns. An architecture for a visual-based PNT alternative. *Acta Astronautica*, 210:601–609, 2023. doi: 10.1016/j.actaastro.2023.05.022. University of Sydney. Visual-based PNT using star tracking + horizon sensing achieves ¡100m for LEO satellites. CROSS star tracker architecture. Maritime requirements: oceanic 1km, coastal 100m, port 1m. Atmospheric offset 25km modeled via EKF. Performance: 50m equivalent ephemeris error. Applicable to LEO GNSS and Lunar navigation infrastructure.

Yuri Dachev and Avgust Panov. 21st century celestial navigation systems. In *Proceedings of the International Scientific Conference*, Varna, Bulgaria, 2017. Classification of celestial navigation methods: traditional manual, traditional computer-based, fully automated. GPS vulnerability analysis (jamming, spoofing, solar weather). Star tracker

technology review (AST-201, CIPP). Sextant accuracy 1-2 arcmin vs star tracker sub-arcsecond. INS/celestial synergy for GPS-denied navigation.

G. D. Dunlap. Major developments in marine navigation during the last 25 years. *NAVIGATION: Journal of The Institute of Navigation*, 18(1):63–76, 1971. doi: 10.1002/j.2161-4296.1971.tb00075.x. Twenty-Fifth Anniversary Issue. Historical survey covering celestial navigation evolution, sight reduction tables (H.O. 214/229), GHA tabulation, quartz chronometers, and submarine periscopic sextant systems.

S. Feldman, P. K. Seidelmann, E. D. Stephenson, and H. C. Kells. Sight reduction using the portable sextant computer system. *Navigation: Journal of The Institute of Navigation*, 19(4):317–321, 1972. doi: 10.1002/j.2161-4296.1972.tb01701.x. U.S. Naval Ordnance Laboratory, U.S. Naval Observatory, Defense Mapping Agency.

Michael J. Garvin. Future of celestial navigation and the ocean-going military navigator. Master's project, Old Dominion University, Norfolk, Virginia, August 2010. URL `https://digitalcommons.odu.edu/ots_masters_projects/41`. Survey of 78 US Army navigators on celestial navigation usage and training viability.

Stanley W. Gery. The direct fix of latitude and longitude from two observed altitudes. *NAVIGATION: Journal of The Institute of Navigation*, 44(1):15–23, 1997. doi: 10.1002/j.2161-4296.1997.tb01935.x.

Robert B. Gordon. The attainment of precision in celestial navigation. *The Journal of Navigation*, 17(2):125–147, 1964. doi: 10.1017/S0373463300032690. Yale University. Controlled experimental study of 500 observations separating error sources. Random error σ=0.33' ideal, 0.70' poor horizon. Systematic errors up to 7' with restricted visibility. Telescope optical quality more important than magnification.

Catherine Hohenkerk, John Kemp, and Brian Nibbs. Astro navigation remembered. *The Journal of Navigation*, 65(3):381–395, 2012. doi: 10.1017/S0373463312000033. HM Nautical Almanac Office, UK Hydrographic Office.

Wayne E. Hoover. Algorithms for confidence circles and ellipses. NOAA Technical Report NOS 107 C&GS 3, National Oceanic and Atmospheric Administration, Rockville, MD, September 1984.

George H. Kaplan. Determining the position of a vessel from celestial observations and motion. *NAVIGATION: Journal of The Institute of Navigation*, 42(4):631–648, 1995. doi: 10.1002/j.2161-4296.1995.tb01911.x. U.S. Naval Observatory, Washington, D.C.

John Karl. *Celestial Navigation in the GPS Age*. Paradise Cay Publications / Celestaire, Arcata, CA / Wichita, KS, revised and expanded edition, 2011. ISBN 978-0-939837-75-7. Comprehensive textbook covering both tabular (H.O. 249, H.O. 229) and

calculator methods. Key equations: sin(Hc)=sin(L)sin(d)+cos(L)cos(d)cos(LHA) for altitude, cos(A)=(sin(d)-sin(L)sin(Hc))/(cos(L)cos(Hc)) for azimuth. Covers altitude corrections (dip, refraction, parallax, semidiameter), St. Hilaire method, lunar distances, special sights (Polaris, meridian). Accuracy discussion: 1-2 nm practical limit. 60 nm per degree conversion. Navigation triangle geometry with worked examples.

Stjepo Kotlarić. Sight reduction — by tables or by celestial navigation computer? *International Hydrographic Review*, LIII(2):123–156, July 1976. Hydrographic Institute of the Yugoslav Navy, Split.

Chong-hui Li, Yong Zheng, Chao Zhang, Yu-Lei Yuan, Yue-Yong Lian, and Pei-Yuan Zhou. Astronomical vessel position determination utilizing the optical super wide angle lens camera. *The Journal of Navigation*, 67(4):633–649, 2014. doi: 10.1017/S0373463314000058. Zhengzhou Institute of Surveying and Mapping, China.

Chong-hui Li, Zhang-lei Chen, Xin-jiang Liu, Bin Chen, Yong Zheng, Shuai Tong, and Ruo-pu Wang. Adaptively robust filtering algorithm for maritime celestial navigation. *The Journal of Navigation*, 75(1):200–212, 2022. doi: 10.1017/S0373463321000758.

Paul McConnell. Slide rules, sextants, and the sky: Instrumentation milestones in aerial celestial navigation. *Journal of the Oughtred Society*, 17(2):40–50, 2008. Historical review of aerial celestial navigation instruments including Bygrave slide rule, bubble sextants, and sight reduction methods.

National Geospatial-Intelligence Agency. *The American Practical Navigator (Bowditch).* National Geospatial-Intelligence Agency, bicentennial edition, 2019. Publication No. 9.

National Geospatial-Intelligence Agency. *Sight Reduction Tables for Marine Navigation.* National Geospatial-Intelligence Agency, 2020. Publication No. 229.

Van-Suong Nguyen and Nam-Kyun Im. Development of computer program for solving astronomical ship position based on circle of equal altitude equation and SVD-least square algorithm. *Journal of Navigation and Port Research*, 38(2):89–96, 2014. doi: 10.5394/KINPR.2014.38.2.89.

Ryan S. Park, William M. Folkner, James G. Williams, and Dale H. Boggs. The JPL planetary and lunar ephemerides DE440 and DE441. *The Astronomical Journal*, 161(3): 105, 2021. doi: 10.3847/1538-3881/abd414. Jet Propulsion Laboratory. Authoritative reference for JPL ephemeris accuracy used by Skyfield. DE440 for modern navigation (1550-2650), DE441 for historical data.

Tony Pinčetić, Zvonimir Lušić, and Paško Esko Krančević. The role of celestial navigation in modern day and future navigation. In *MT'24: 10th International Conference on*

Maritime Transport, pages 1–11, Barcelona, Spain, June 2024. Universitat Politècnica de Catalunya. University of Split. STCW/IMO regulatory review and SWOT analysis. Celestial navigation remains only real alternative to GNSS. Norway 2008 proposed cancellation; China proposed simplification; US maintains as GPS backup. SOLAS V/19 inconsistency: sextant not required onboard.

Tyler G. R. Reid, Bryan Chan, Ashish Goel, Kazuma Gunning, Brian Manning, Jerami Martin, Andrew Neish, Adrien Perkins, and Paul Tarantino. Satellite navigation for the age of autonomy. In *2020 IEEE/ION Position, Location and Navigation Symposium (PLANS)*, San Mateo, CA, 2020. Xona Space Systems. Historical navigation accuracy trend: 10x improvement every 30 years (celestial km-level 1900s, LORAN 100s m 1940s, Transit 10s m 1964, GPS m 1995, decimeter 2020s). Autonomous vehicles require 10 cm (95%) highway, 5 cm city. GPS vulnerabilities: 50,000+ disruptions Europe 2016-2018, Tesla spoofing 2019. LEO navigation proposed for autonomy.

Brandon Rhodes. Skyfield: High precision research-grade positions for planets and earth satellites generator, 2023. URL `https://rhodesmill.org/skyfield/`. Python package for astronomical computations.

Paul F. Ross. Minimizing errors in celestial positioning. *NAVIGATION: Journal of The Institute of Navigation*, 41(3):251–264, 1994. doi: 10.1002/j.2161-4296.1994.tb01879.x. Charles River Power Squadron. Statistical analysis of sextant error sources: index error (2.0'), personal random error (0.5'), timing, prismatic error. Total error 2.1' reducible to 0.5' with proper procedures.

P. K. Seidelmann, P. M. Janiczek, and R. F. Haupt. The almanacs—yesterday, today and tomorrow. *NAVIGATION: Journal of The Institute of Navigation*, 24(4):303–312, 1976. doi: 10.1002/j.2161-4296.1976.tb00755.x. U.S. Naval Observatory. Evolution of nautical almanacs and introduction of Almanac for Computers with Chebyshev polynomials.

Joel Silverberg. Circles of illumination, parallels of equal altitude, and le calcul du point observé: Nineteenth century advances in celestial navigation. In *Proceedings of the Canadian Society for the History and Philosophy of Mathematics*, Montréal, Québec, July 2007. Concordia University.

E. Myles Standish and Agnès Fienga. Accuracy limit of modern ephemerides imposed by the uncertainties in asteroid masses. *Astronomy & Astrophysics*, 384:322–328, 2002. doi: 10.1051/0004-6361:20011821. JPL and IMCCE. Monte Carlo analysis of ephemeris uncertainty from asteroid mass errors. Earth-Mars ephemeris uncertainty 2-5 km over decades.

Peter F. Swaszek, Richard J. Hartnett, and Kelly C. Seals. Rethinking star selection in celestial navigation. In *Proceedings of the 2019 International Technical Meeting of The Institute of Navigation*, pages 522–535, Reston, Virginia, January 2019. Institute of Navigation. doi: 10.33012/2019.16678. University of Rhode Island and U.S. Coast Guard Academy.

USNO and HMNAO. *The Nautical Almanac*. US Government Publishing Office, 2025. Annual publication by United States Naval Observatory and Her Majesty's Nautical Almanac Office.

Shujie Yang, Wuwei Feng, Shuai Wang, and Jing Li. A SINS/CNS integrated navigation scheme with improved mathematical horizon reference. *Measurement*, 195:111028, 2022. doi: 10.1016/j.measurement.2022.111028.

Pawel Zalewski, Andrzej Bak, and Michael Bergmann. Evolution of maritime GNSS and RNSS performance standards. *Remote Sensing*, 14(21):5291, 2022. doi: 10.3390/rs14215291. Maritime University of Szczecin and BM Bergmann-Marine. Comprehensive review of IMO GNSS performance standards evolution. Key parameters: 10m accuracy (95%), 25m alert limit, 10s time-to-alarm, 10^{-5} integrity risk per 3h. Shows protection levels can exceed alert limits. SWOT analysis identifies jamming/spoofing vulnerabilities. Establishes need for backup navigation systems.